

## Article

# Core Orientation Technology Based on Drilling Trajectory Projection and Its Application in In Situ Stress Measurement of the Deepest Shaft in China

Chunde Ma <sup>1,2</sup>, Guanshuang Tan <sup>1</sup>, Xibing Li <sup>1</sup>, Jiaqing Xu <sup>1</sup>  and Jiangzhan Chen <sup>1,\*</sup> 

<sup>1</sup> School of Resources and Safety Engineering, Central South University, Changsha 410083, China; cdma@csu.edu.cn (C.M.); tanguanshuang@csu.edu.cn (G.T.); xbli@csu.edu.cn (X.L.); xu1001@csu.edu.cn (J.X.)

<sup>2</sup> Advanced Research Center, Central South University, Changsha 410083, China

\* Correspondence: jiangzhanchen@csu.edu.cn

**Abstract:** Deep borehole cores are an important material basis for understanding deep stress conditions and rockburst risk; however, the complex environment of deep boreholes poses many challenges to traditional core orientation techniques, thus limiting the application of cores in fields such as in situ stress measurement. A technical method of restoring the original spatial attitude of nonoriented geological cores on the ground was proposed based on the inherent “trajectory projection consistency” relationship between the borehole and the corresponding core. A prototype machine of core ground reorientation was developed. Using this method and machine, ground reorientation was performed on cores drilled from the deepest shaft in China. Subsequently, the reoriented core acoustic emission (AE) method was conducted to identify the in situ stress within the project area. Meanwhile, measurement accuracy was verified by the stress relief method. The results show that the in situ stress distributions, including the azimuth and the trends in principal stresses by the two methods, are in good agreement and indicate that the historical maximum principal stress in the case of the mine has little abrupt variability with that of the present day. The research results can be used as the design basis for the safe construction of the deepest shaft.

**Keywords:** core orientation; in situ stress measurement; acoustic emission; stress relief; deep borehole



**Citation:** Ma, C.; Tan, G.; Li, X.; Xu, J.; Chen, J. Core Orientation Technology Based on Drilling Trajectory Projection and Its Application in In Situ Stress Measurement of the Deepest Shaft in China. *Minerals* **2022**, *12*, 521. <https://doi.org/10.3390/min12050521>

Academic Editors: Anye Cao, Zhenlei Li and Abbas Taheri

Received: 10 March 2022

Accepted: 20 April 2022

Published: 22 April 2022

**Publisher's Note:** MDPI stays neutral with regard to jurisdictional claims in published maps and institutional affiliations.



**Copyright:** © 2022 by the authors. Licensee MDPI, Basel, Switzerland. This article is an open access article distributed under the terms and conditions of the Creative Commons Attribution (CC BY) license (<https://creativecommons.org/licenses/by/4.0/>).

## 1. Introduction

In recent years, the exploitation of mineral resources in most countries has gradually moved to greater depths (from 1 to 5 km) [1,2]. With the increase in mining depth, high in situ stress generates an increased risk of rockburst and seismicity [3] and brings significant challenges to the excavation and support of engineering structures [4–9]. To understand the distribution of stress conditions and the possibility of rockburst in the crust for the scientific design and excavation of deep engineering structures, it is necessary to conduct deep in situ stress measurement [10–14].

In the process of in situ stress measurement, deep geological drilling is a necessary tool to obtain measurement space and rock cores to understand information about the deep strata [15,16]. In particular, the drilled rock core is the material basis that must be collected for geological research and mineral exploration. In the past, only sufficient sampling rate and representativeness of the core were required, regardless of its true orientation, so the cores extracted were mostly nonoriented [17,18]. However, in modern refined underground engineering research, it is sometimes required to collect oriented cores or reorient the cores on the ground [19,20]. The so-called oriented core is extracted from the bottom of the borehole and can be restored to its original underground spatial orientation. After the original orientation of the core is determined, not only can the occurrence information of geological structures (including faults, joints, schisms, crevices,

and other planar structures) be acquired [21], but geological characteristics such as tectonic stress fields can also be obtained.

Core orientation is difficult. For many years, many scientific and technical personnel have been exploring precise, simple, convenient, and economical orientation techniques. The main methods at present are: (1) Oriented core barrel technology uses a scoring tool to cut three V-shaped grooves in the core, and a camera on the scoring tool cooperates with a magnetic compass to read the direction of the grooves [21,22]. A basic requirement of this method is that a nonmagnetic drill bit must be used (to avoid interference with the magnetic compass). In addition, the orientation accuracy of this method also depends on the curvature of the groove [23]. (2) The dipmeter orientation method is oriented by the direction of the maximum inclination of the strata appearing within the core [22]. The prerequisite for the application of this technique is that there must be an identifiable structural surface on the core, and its dip angle must be steep enough. If the dip angle of the structure is horizontal or close to horizontal and the borehole is vertical, the original spatial orientation of the core cannot be determined. (3) The borehole imaging orientation method refers to the use of special instruments to obtain features on the borehole wall [24–29], and compare the feature with the drilled core, to achieve core reorientation [30,31]. However, this technique requires a set of specialized, expensive instruments and warrants professionals to perform operations in the borehole. Its orientation accuracy depends on the cleanliness of the borehole wall and the clarity of the image obtained by the instrument. (4) The paleomagnetic orientation method is aimed at obtaining the viscous remanence component before and after demagnetization by thermal demagnetization or alternating-current demagnetization [32–35]. The coordinates of the core are converted to geographic coordinates, and the direction of the viscous remnant magnetic component is compared with the direction of the magnetic field in the geographic coordinate system to complete core orientation [36]. The particular advantage of the paleomagnetic orientation method is that reorientation can be achieved using only the core itself [32].

Oriented cores play many roles in geological engineering practice and become an important support for in situ stress measurement [37,38]. Therefore, many scholars have suggested core-based methods to estimate the magnitude and orientation of in situ stress, one of which is the acoustic emission (AE) method [37,39–44]. The AE method has the advantages of low cost, strong controllability, and less restrictive conditions [41,45,46]. Provided that a core from a certain depth can be obtained, in situ stress testing can be conducted; however, the AE method requires a known spatial orientation of the core to perform in situ stress measurement. The existing core orientation technique has disadvantages such as high cost and complex operation, which results in many deep cores that cannot be oriented, thus limiting the widespread application of core-based methods such as the AE method.

In this study, based on the inherent essential relationship between geological drilling and cores, a new core orientation method combining drilling trajectory projection and rotation calibration was proposed. Using this method and the developed prototype machine, ground reorientation was performed on cores drilled from –950 to –1550 m in the deepest shaft in China. Furthermore, in situ stress measurement was carried out by combining the reoriented cores with the AE method, and the measurement results were verified by the stress relief method. This research innovation could provide a solution for measuring in situ stress based on deep nonoriented cores.

## 2. Drilling Trajectory Projection and Core Orientation Technology

### 2.1. Theoretical Basis

#### (1) Absolute bending principle of drilling trajectory

In the process of conventional core drilling construction, the drilling process of the bit will be affected by geological and technological factors, and the drilling trajectory often deviates from the pre-set trajectory. In the traditional sense, the straightness of straight boreholes is only a relative straightness that ignores the influences of the inclination

accuracy error and the measurement density, while the bending of the drilling trajectory curve is absolute. That is, provided the accuracy of the measuring instrument (borehole inclinometer) is sufficient, the small change values of the apex and azimuth angles on the borehole trajectory can be measured, and the bending change of the borehole in space is determined.

(2) Consistent bending principle of drilling trajectory and core axis

The current core drilling generally uses diamond or cemented carbide annular drilling tools, which are rotated in the rock formation to obtain the core. In this way, the borehole and the corresponding core are always concentric cylinders with a common axis, and the drilling trajectory and core axis are coincident in spatial coordinates. Due to the drilling trajectory showing a gradual and continuous change from the upper end to the lower end, the deformations of the borehole and the core exhibit consistent bending characteristics.

(3) Uniqueness principle of matching the spatial attitude of the borehole and the core

The axis of the borehole coincides with the axis of the core, and the trajectory of its axis is a changing spatial curve. Even for a short section of the core, the tilt or bending parameters (including depth, apex angle, and azimuth angle) of each point on the axis trajectory are different in space. If the core is restored to the original posture in the borehole, the apex and azimuth angles of each point on the borehole axis and the corresponding core axis must be the same, which means that the borehole axis and its corresponding core axis match uniquely in three-dimensional space.

## 2.2. Establishment of Drill-Core Spatial Attitude Model

Based on the above principles, a physical model of borehole-core bending space attitude is established (Figure 1). The model is described thus: a borehole is drilled from top to bottom in the rock formation, and at the same time concentric core pillars with overlapping axis trajectories (due to rock structure, joints, cracks, and recurrences, the core pillars will break and decompose into several small core sections) are obtained. The borehole is affected by some external factors during the drilling process, and its actual trajectory deviates slightly from the pre-set trajectory. The space curve CD in Figure 1 is the characteristic trajectory of the axis that characterizes the bending of the borehole. The changing values of apex angle and azimuth angle can be determined by a high-precision borehole inclinometer. Two points O and O' on the spatial curve CD are taken, and their tangents are drawn through these two points. In this way, the angle between the tangent and the vertical is the apex angle, and the angle between the tangent and the north line after being projected on the horizontal plane is the azimuth angle, so the azimuth and apex angles of points O and O' are  $(\alpha_1, \theta_1)$  and  $(\alpha_2, \theta_2)$ . The apex and azimuth angles of the two points on the axis track change; that is, the borehole is bent.

The core axis trajectory coincides with the drilling trajectory, so the core is bent in line with the borehole. The bending parameters of the borehole axis trajectory can be measured using a dedicated borehole inclinometer, but because the axis of the core is hidden within the core, it is not easy to use the instrument directly to measure the bending accurately and make obvious direction markings. Therefore, how to elucidate the bending feature of the core axis on the surface of the core will be discussed below.

According to the actual drilling conditions, the three-dimensional drilling trajectory can be considered as the connection of two-dimensional line segments in the countless azimuth planes ( $\alpha_1 \approx \alpha_2$ ). Taking the core drilling at a certain depth and azimuth as an example, the drill bit at the bottom of the hole is mainly subject to the combined effect of drilling force (along the axial direction  $F_A$ ) and increasing-inclination (or decreasing-inclination) force (along the radial direction  $F_R$ ) during the drilling process without considering the rotating state [47]. The combined active force leads to the bending of the drilling trajectory, and the actual drilling trajectory of the borehole can be divided into increasing-inclination or decreasing-inclination states, as shown in Figure 2. Further, as the bit is drilled from axis sections A-A' to B-B' of a borehole, the borehole axis (core axis) is bent within the 2D

intersection plane of forces  $F_R$  and  $F_A$ . The shortest drilling arc ( $L_{min}$ ) and a longest drilling arc ( $L_{max}$ ) are formed on the core surface in the moving paths of the combined active force, and the direction of arcs  $L_{min}$  and  $L_{max}$  is consistent with the drilling direction.

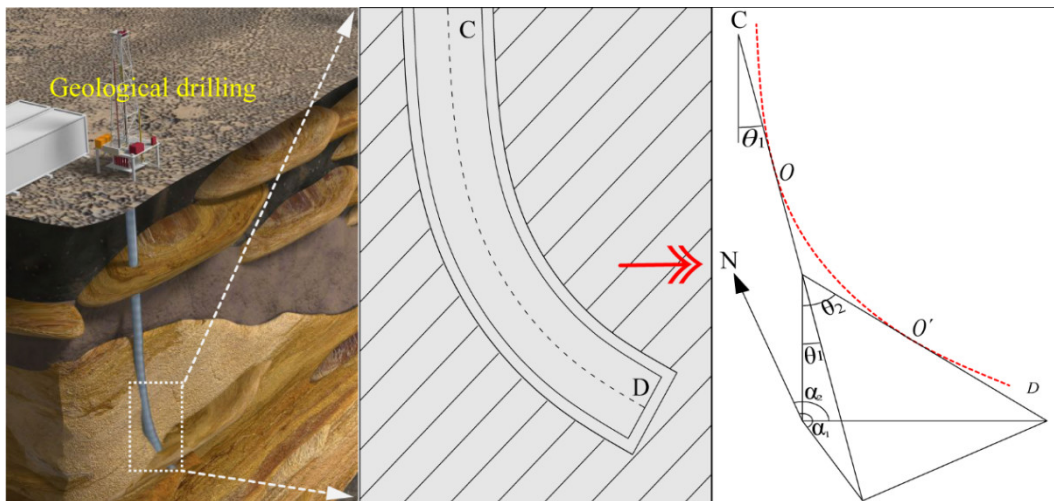


Figure 1. Schematic diagram of drilling-core spatial geometry model ( $\theta_1$ : apex angle of point O;  $\theta_2$ : apex angle of point O';  $\alpha_1$ : azimuth angle of point O;  $\alpha_2$ : azimuth angle of point O').

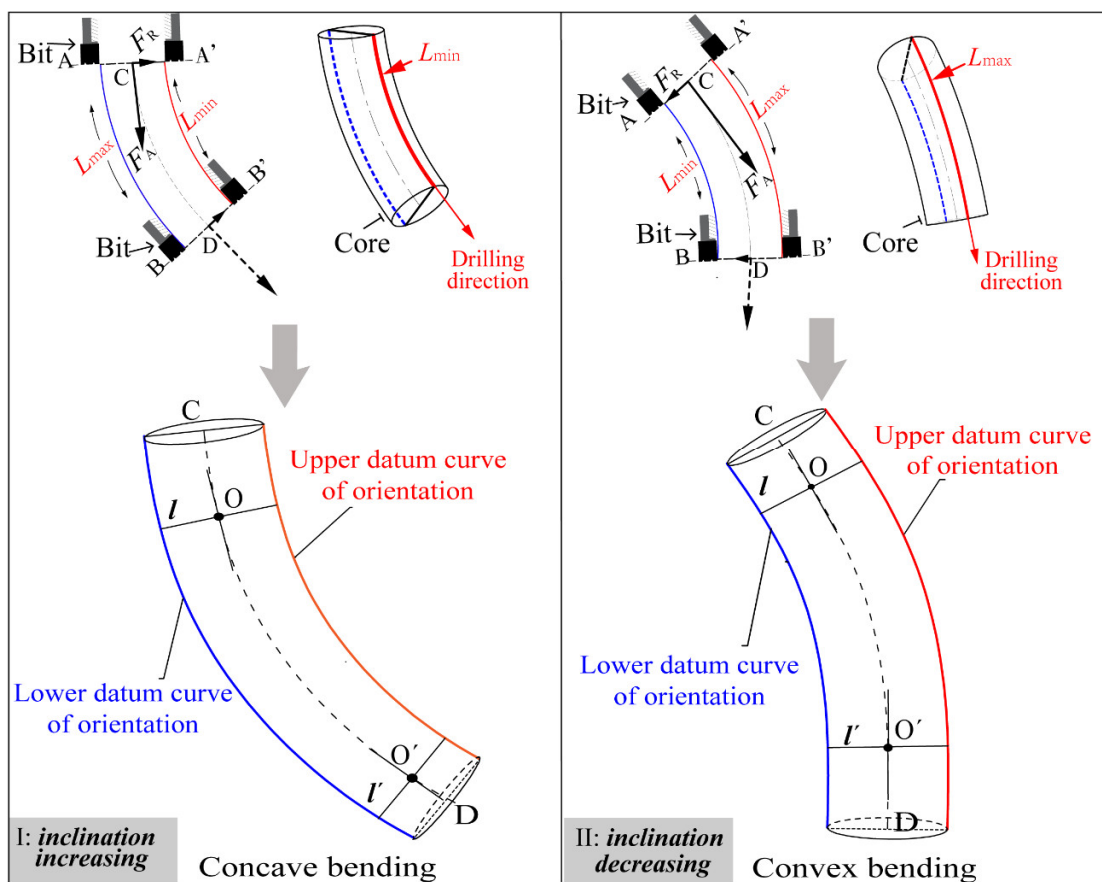


Figure 2. Spatial relationship between the datum curve of the orientation and the core bending feature ( $F_A$ : drilling force along the axial direction;  $F_R$ : force along the radial direction;  $L_{min}$ : shortest drilling arc;  $L_{max}$ : longest drilling arc).

As shown in Figure 2, the normal lines  $l$  and  $l'$ , passing through points  $O$  and  $O'$  respectively, are perpendicular to the tangent of the drilling direction in the 2D intersection plane of forces  $F_R$  and  $F_A$ . The normal line and the outer surface of the core produce two intersection points, which are the intersection of the cutting circle of bit and the combined active force plane. Similarly, the same method is used to cross each point on the CD to make the normal line, and the intersection point is produced with the outer surface of the core. Then, the two sets of intersection points on both sides of the core are connected into bending curves. The bending curves on the core surface are parallel to the drilling trajectory and are located on the same spatial surface, which can represent the bending characteristics of the core, as does the drilling trajectory (herein, they are referred to as the datum curve of the orientation). According to the changing trend of the apex angle of each point on the datum curve, it can be defined: from top to bottom, if the apex angle changes from small to large, the core bending feature is defined as concave; if the apex angle changes from large to small, then the core bending feature is defined as convex. According to the definition of the spatial azimuth, regardless of the concave or convex type, the upper datum curve of the orientation rotates its own azimuth value counterclockwise and coincides with the north line (the azimuth value of the lower datum curve is different from that of the upper datum curve by  $180^\circ$ ).

The method for determining this directional reference generatrix on the surface of the core is described below. As shown in Figure 3, passing through points  $O$  and  $O'$  on the core axis trajectory, two normal cross-section circles are cut from the core, namely circles  $O$  and  $O'$ . Their dip angles are equal to the apex angles ( $\theta_1, \theta_2$ ) of the center points, and the azimuth angles are  $\alpha_1$  and  $\alpha_2$ , respectively. We project the circle  $O'$  onto the plane where circle  $O$  is located, and the center of the two circles will deviate with an offset angle ( $\alpha_1 - \alpha_2 \approx 0$ ). At this time, the concentricity correction rotation method is used to rotate the projection of circle  $O'$  projection around  $O$ . The displacement detection point  $N$  is set on the outside, and the displacement data of each point on the surface of the core are synchronously recorded when the core is rotating. According to the displacement data, the maximum displacement point  $E$  and the minimum displacement point  $F$  can be determined (the intersection of the extension line of points  $O$  and  $O'$  and the projection of circle  $O'$  projection can draw the largest and smallest radius circles, respectively), the corresponding rotation angle is recorded, and points  $E$  and  $F$  on the core are marked. Then, the position of the displacement detection point  $N$  is changed along the core drilling direction, and the core is rotated and measured multiple times to attain multiple sets of maximum displacement points and minimum displacement points on the outer surface of the core. Two datum curves of the orientation can be identified by connecting all the points with the maximum displacement and the points with the minimum displacement. According to the principle of plane projection, the azimuth angle of the upper datum curve is the same as the azimuth angle of the core section. The core is rotated to rotate the upper datum curve counterclockwise by an azimuth angle. Then, the line on the core corresponding to the rotated upper datum curve is the north line. This orientation (north line) is marked to complete the ground reorientation of the core.

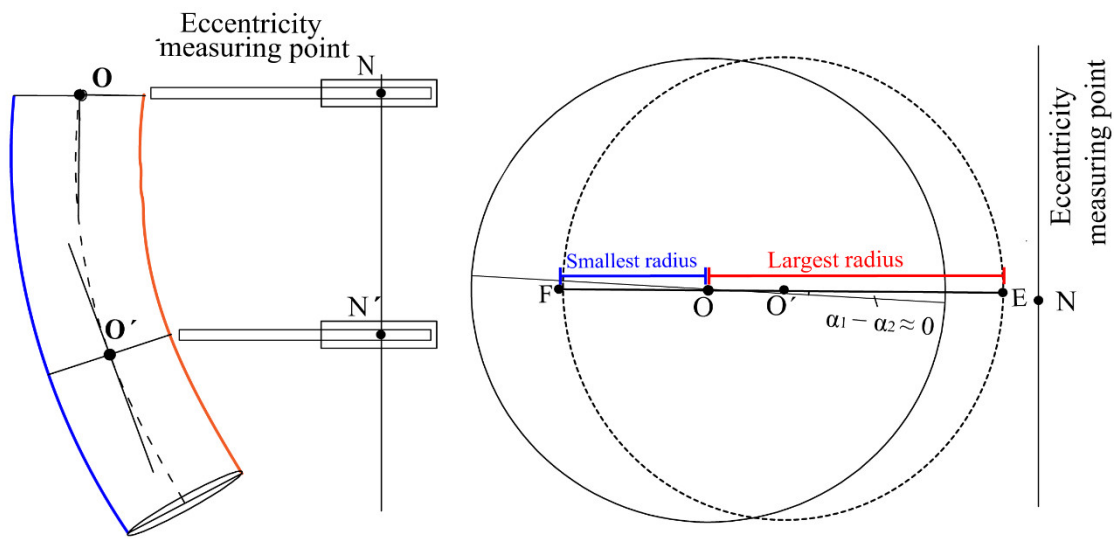


Figure 3. Projection of circle  $O'$  on the plane of circle  $O$ .

### 3. Implementation of Drilling Trajectory Projection and Core Orientation Technology

#### 3.1. Development of the Core Orientation System

A ground orientation test system was established according to the theory of drilling trajectory projection and core orientation technology, as shown in Figure 4. This system mainly consists of a rotary chuck, core clamping jaws, metal base, displacement sensor, laser indicator light, monitoring device, and test computer. After the test system was established, its angle was calibrated to ensure that the rotation angle of the rotary chuck was synchronized with the displacement monitoring software (YXW-0, Central South University, Changsha, China).

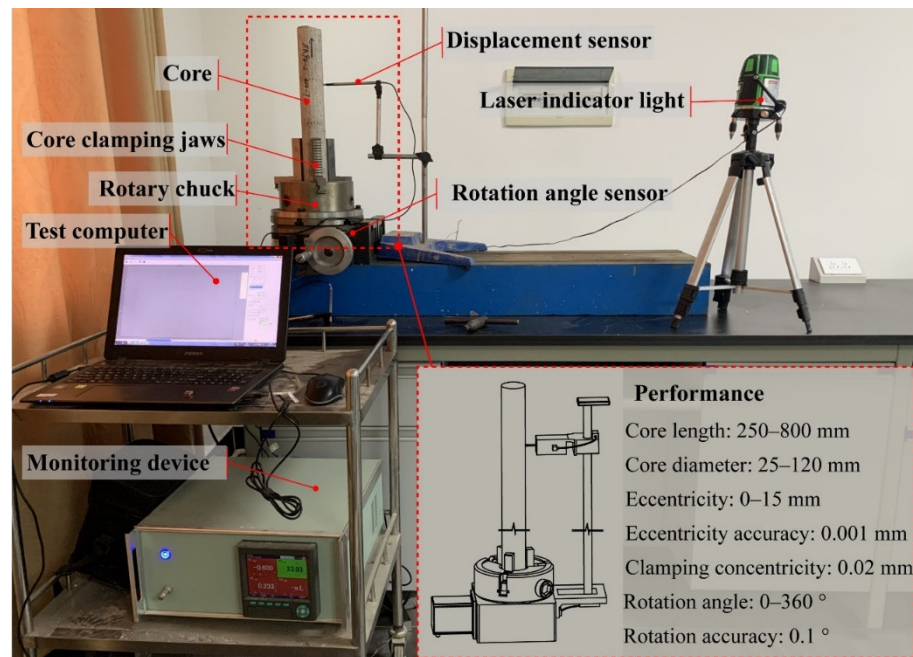


Figure 4. Ground orientation test system.

#### 3.2. Method and Process of Core Orientation

Using the core orientation system to orient geological cores, the steps are described as follows:

- (1) We connected the test system, screwed the claw on the rotary chuck, and clamped the core so that the axis of the upper-end face of the core coincided with the axis of the chuck. Then, the displacement sensor was closed to the core surface, the displacement and rotation angle monitoring software was opened, and the rotary chuck handle was shaken to drive the core to rotate from the initial position. The displacement measuring device synchronously measured the displacement data of each point on the core surface relative to the chuck axis during the rotation of the core.
- (2) The software was employed to solve the displacement peak point and valley point, and the corresponding rotation angle of the peak point and valley point on the rotary chuck (the angle scale was engraved on the rotary chuck) was recorded. When the displacement reached the peak point and valley point, the contact point between the spherical probe of the displacement sensor and the core surface was marked.
- (3) Multiple displacement peak points and displacement valley points can be obtained by changing the position of the displacement sensor relative to the core and making multiple measurements. Connecting these points can obtain two marking lines: one is the upper datum curve of the orientation, and the other is the lower datum curve of the orientation.
- (4) The laser indicator can shoot a vertical beam of light; we aimed it at the core and illuminated the corresponding datum curve. Then, we rotated the upper datum curve to the counterclockwise direction by an azimuth angle. Thus, the light shining on the core by the laser indicator is the north (N) line. This line was marked, and the core was oriented.

#### 4. In Situ Stress Measurement by Reoriented Cores AE Method

The essence of AE is the closure or expansion of microdefects in the rock under the action of external load. When the rock is stressed, microcracks corresponding to the magnitude and direction of the applied load are generated. When the force on the rock again is less than the force that caused the crack earlier, the crack or defect will not develop further, and fewer AE events will be stimulated. Once the stress on the rock reaches or exceeds the earlier stress, the crack or defect will expand, and a large number of AE events will occur (the Kaiser effect [48]). The turning point from low AE to high AE is called the Kaiser effect point, and the stress corresponding thereto is the maximum stress previously experienced by the rock. Using this feature, test specimens are processed in multiple directions to determine the stress corresponding to the sudden increase in AE, which is then combined with the calculation formula to obtain the three-dimensional in situ stress.

##### 4.1. Sample Preparation and Experimental Equipment

The core samples for the in situ stress test were taken from the JCK-1 deep geological borehole (−1550 m) near the new main shaft of Xincheng Gold Mine in Shandong, China. The design depth of the new main shaft is 1527 m, and the diameter of the shaft is 7.5 m. After completion, it will become the deepest shaft in China. At present, there are still a series of technical bottlenecks in the construction of deep shafts below 1500 m. The rockburst induced by high in situ stress is one of the most prominent problems. To measure the in situ stress of the deepest shaft, seven measurement points at different depths such as −950 m, −1050 m, −1150 m, −1250 m, −1350 m, −1450 m, and −1550 m were selected, and deep nonoriented cores were collected, as shown in Figure 5. In order to ensure the accuracy of the orientation, we carried out the following work during the core preparation process. First, during operation in the field, a wireless digital compass inclinometer was usually used to measure the borehole inclination per 10 cm, enabling an accurate description of the drilling trajectory. Then, only the cores with homogeneous lithology and integrity structure were selected as test specimens, which usually suffer from small local variations of stress and normal deformation recovery. In addition, during the reorientation process, the accuracy of the core feature data was judged by checking the azimuth deviation between

the upper datum curve of the orientation and the lower datum curve of the orientation, and only the cores that met the deviation requirements were selected for reorientation.

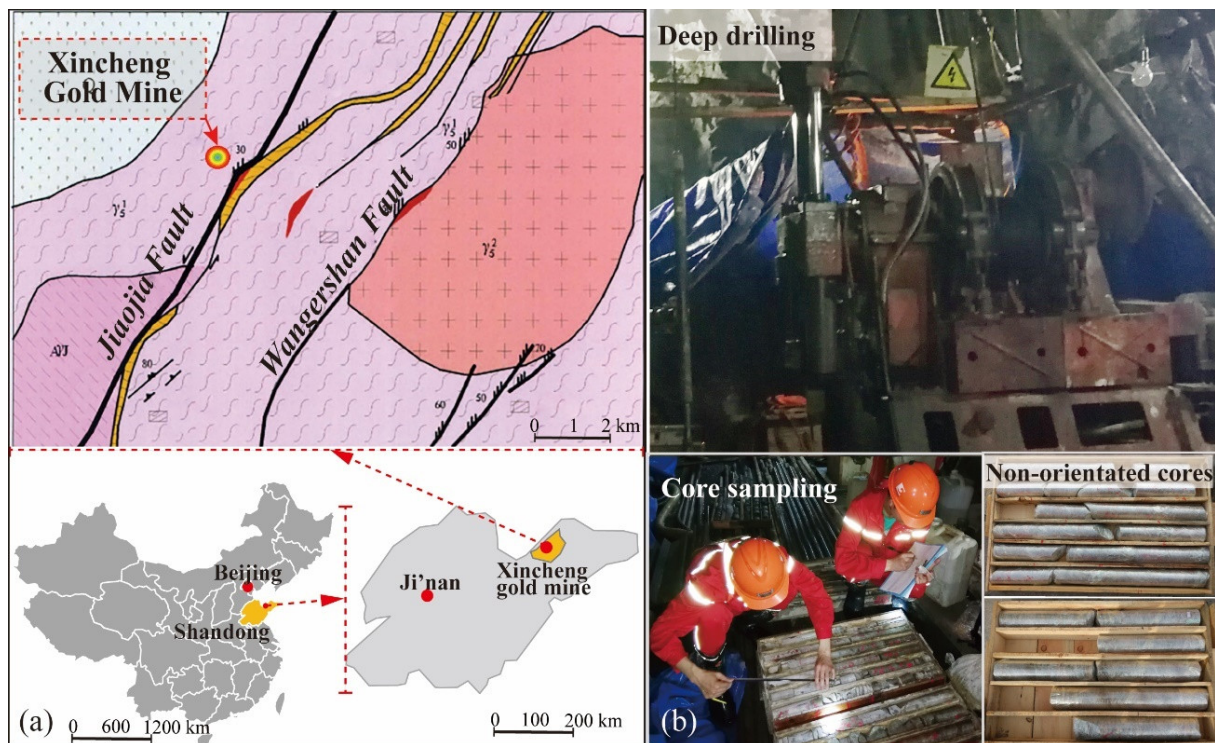


**Figure 5.** Core sampling at in situ stress measurement area: (a) geographic location; (b) nonoriented core sampling.

After the reorientation of the core according to Section 3, the suitability of the geological setting and the core properties were evaluated, and the circumferential P-wave velocity measurements were carried out on cores at different depths using the AST function of the AE instrument. Based on the above results, it was roughly determined that the main direction of the regional historical in situ stress is the east–west direction, which is used to guide the sampling direction of the AE specimens. Then, we drilled three or four small cylindrical specimens measuring 25 mm in diameter × 50 mm in height, oriented at  $V$ ,  $0^\circ$ ,  $45^\circ$ , and  $90^\circ$ , as shown in Figure 6. Each specimen was finely polished to the required flatness.

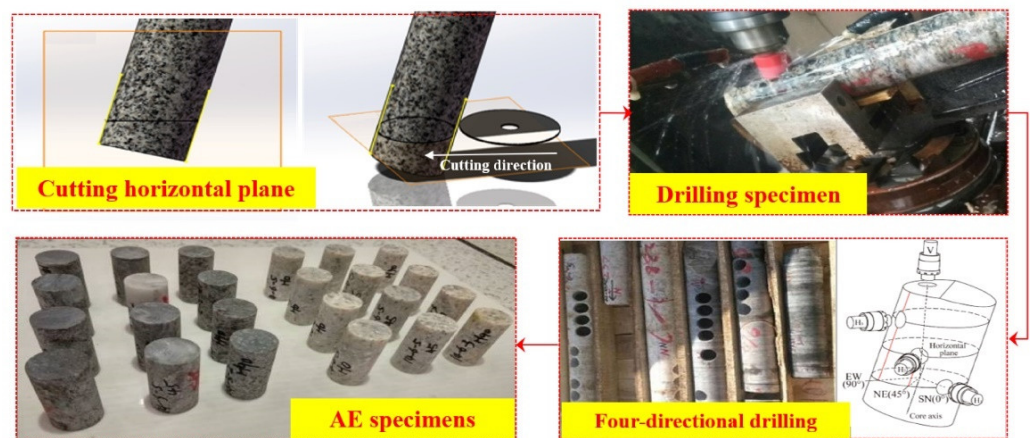


**Figure 6.** Schematic representation of the drilling of cylindrical specimens.

The MTS815 rock material testing machine that can provide a maximum axial load of 2600 kN was used. In addition, it was also equipped with the American PCI-2 AE test system. The load and displacement data of the MTS815 testing machine were introduced into the AE test system as external parameter signals. After debugging the two data streams, the load and AE data were acquired simultaneously, which is convenient when identifying the Kaiser point, as shown in Figure 7.

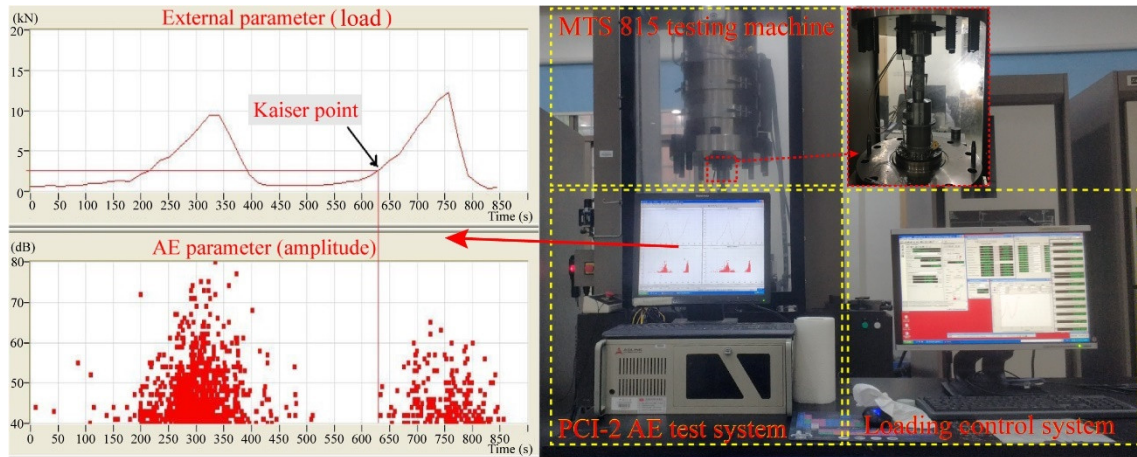


Figure 7. Test equipment and AE test data.

#### 4.2. Test Scheme

The loading and unloading tests on the specimens were conducted based on the incomplete erasure phenomenon of AE activities [49]. When loading, the displacement control mode was adopted; the displacement rate was set to 0.12 mm/min, and that during unloading was set to 0.35 mm/min. The maximum stress imposed by the first loading regime was higher than the estimated value of the original stress on the rock. Two AE probes were used, which were fixed on the axisymmetric sides of the specimen for dual-channel AE signal acquisition. The contact surface between the probe and the rock specimen was coated with petroleum jelly. The contact surface of the loading head was also coated with petroleum jelly to reduce the noise generated by the end effect. The noise threshold of the AE test system was set to 45 dB, and the AE data acquisition frequency was set to 1 MHz.

#### 4.3. Test Results

According to the test method above, a comprehensive analysis for determining the Kaiser stress was performed with the tangent method [50,51], and the corresponding Kaiser effect point of the rock specimen was obtained, as shown in Table 1 after sorting.

The stress applied at the Kaiser point in the vertical direction is regarded as the in situ stress in the vertical direction of the point. The magnitude and direction of the maximum horizontal principal stress and the minimum horizontal principal stress are calculated based on the analysis of plane stress state [52]. It is assumed that the normal and shear stresses on a core section are  $\sigma_\beta$  and  $\tau_\beta$ . The angle between the direction of  $\sigma_\beta$  and the north direction is  $\beta$ . The direction of normal compressive stress is positive. Thus, the following equilibrium equations can be established:

$$\begin{cases} \sigma_\beta dS + (\tau_{EN} dS \sin \beta) \cos \beta - (\sigma_E dS \sin \beta) \sin \beta + (\tau_{NE} dS \cos \beta) \sin \beta - (\sigma_N dS \cos \beta) \cos \beta = 0 \\ \tau_\beta dS - (\tau_{EN} dS \sin \beta) \sin \beta - (\sigma_E dS \sin \beta) \cos \beta + (\tau_{NE} dS \cos \beta) \cos \beta + (\sigma_N dS \cos \beta) \sin \beta = 0 \end{cases} \quad (1)$$

where  $\sigma_N$  is the Kaiser point stress in the north direction ( $0^\circ$ ),  $\sigma_E$  is the Kaiser point stress in the east direction ( $90^\circ$ ),  $\tau_{EN}$  is the shear stress in the east–north direction, and  $\tau_{NE}$  is the shear stress in the north–east direction.

Table 1. Kaiser effect point result.

Drilling Depth (m)	Kaiser Point Stress in the Vertical Direction (Mpa)		Kaiser Point Stress in the Horizontal Direction (MPa)					
			$\sigma_N$ (0°)		$\sigma_{NE}$ (45°)		$\sigma_E$ (90°)	
	Actual Value	Average Value	Actual Value	Average Value	Actual Value	Average Value	Actual Value	Average Value
−950	26.61	26.41	14.91	15.52	19.45	19.48	32.95	31.78
	26.45		15.51		18.19		29.93	
	26.18		16.11		20.87		29.27	
	—		15.55		19.43		34.96	
−1050	28.01	29.22	17.76	18.56	24.41	23.83	40.32	40.45
	30.66		17.68		24.36		41.65	
	29.00		19.74		23.65		40.06	
	—		19.07		22.89		39.75	
−1150	32.49	33.33	16.32	16.82	24.25	24.15	36.71	35.19
	33.13		18.91		23.74		37.73	
	34.36		17.44		24.58		34.45	
	—		14.63		24.01		31.85	
−1250	34.21	34.25	19.28	19.49	20.03	20.73	37.61	36.30
	35.19		17.99		23.30		36.44	
	33.36		19.36		18.93		36.89	
	—		21.34		20.66		34.28	
−1350	36.84	35.98	18.71	18.20	23.43	22.47	37.33	39.48
	35.43		19.86		21.55		38.82	
	35.68		16.31		20.79		40.68	
	—		17.91		24.14		41.09	
−1450	40.51	40.01	17.96	17.54	17.38	18.31	34.88	37.11
	40.05		20.30		16.62		35.07	
	39.46		16.19		20.85		39.24	
	—		15.72		18.39		39.24	
−1550	42.01	40.95	23.91	19.16	21.09	22.72	37.61	43.17
	40.84		20.05		22.62		45.65	
	40.02		15.30		19.38		43.84	
	—		17.37		27.79		45.57	

According to the equality theorem of shear stress, the values of  $\tau_{EN}$  and  $\tau_{NE}$  are equal, and Equation (1) can be simplified to Equation (2) as follows:

$$\begin{cases} \sigma_\beta = \frac{\sigma_N + \sigma_E}{2} + \frac{\sigma_N - \sigma_E}{2} \cos 2\beta - \tau_{EN} \sin 2\beta \\ \tau_\beta = \frac{\sigma_E - \sigma_N}{2} \sin 2\beta - \tau_{EN} \cos 2\beta \end{cases} \quad (2)$$

According to the definition of the maximum and minimum principal stress, the shear stress  $\tau_\beta$  on the principal plane is 0. Therefore, the angle of the principal stress can be determined according to Equation (3) as follows:

$$\tan 2\beta = \frac{2\tau_{EN}}{\sigma_E - \sigma_N} \quad (3)$$

After substituting the three-directional Kaiser point stress, Equation (2) can be simplified as follows:

$$\tau_{EN} = \frac{\sigma_N - 2\sigma_{NE} + \sigma_E}{2} \quad (4)$$

where  $\sigma_{NE}$  is the Kaiser point stress in the north–east direction (45°).

By combining Equation (3) with Equation (4), the following can be obtained:

$$\tan 2\beta = \frac{\sigma_N - 2\sigma_{NE} + \sigma_E}{\sigma_E - \sigma_N} \quad (5)$$

The solutions of Equation (5) are the directions of the maximum and minimum principal stresses as follows:

$$\beta = \begin{cases} \frac{\arctan(\frac{\sigma_N - 2\sigma_{NE} + \sigma_E}{\sigma_E - \sigma_N})}{2} \\ 90 + \frac{\arctan(\frac{\sigma_N - 2\sigma_{NE} + \sigma_E}{\sigma_E - \sigma_N})}{2} \end{cases} \quad (6)$$

After substituting the above solutions into Equation (2), the specific values of the maximum and minimum principal stress can be obtained.

$$\left. \begin{matrix} \sigma_H \\ \sigma_h \end{matrix} \right\} = \frac{\sigma_N + \sigma_E}{2} + \frac{\sigma_N - \sigma_E}{2} \cos 2\beta - \frac{\sigma_N - 2\sigma_{NE} + \sigma_E}{2} \sin 2\beta \quad (7)$$

where  $\sigma_H$  is the maximum horizontal principal stress,  $\sigma_h$  is the minimum horizontal principal stress, and  $\beta$  is the angle between the azimuth of the maximum horizontal principal stress and the north direction.

The calculated results are summarized in Table 2.

**Table 2.** In situ stress test results.

Measuring Point Depth (m)	Vertical Principal Stress $\sigma_v$ (MPa)	Self-Weight Stress $\sigma_z$ (MPa)	Maximum Horizontal Principal Stress $\sigma_H$ (MPa)	Minimum Horizontal Principal Stress $\sigma_h$ (MPa)	Azimuth Angle of Maximum Horizontal Principal Stress $\beta$ (°)
−950	26.41	26.46	32.78	14.52	283.57
−1050	29.22	29.16	41.83	17.18	283.70
−1150	33.33	31.86	35.37	16.64	275.72
−1250	34.25	34.56	38.95	16.85	290.22
−1350	35.98	37.26	41.23	16.44	285.43
−1450	40.01	39.96	40.63	14.02	291.33
−1550	40.95	42.66	45.84	17.56	287.55

#### 4.4. Distribution of In Situ Stress

- (1) The vertical principal stress increases nearly linearly with the increase in borehole depth, which is consistent with the self-weight stress at that burial depth (Figure 8a).
- (2) The directions of the maximum horizontal principal stress at different depths are similar, ranging from 275.72° to 291.33° (Figure 8b).
- (3) The in situ stress in the area in which the borehole is located is mainly horizontal tectonic stress. In different soundings of the borehole, the maximum stress is the maximum horizontal principal stress, and the intermediate principal stress is the vertical stress. With the further increase in drilling depth, the dominant role of the horizontal tectonic stress field decreases, and the self-weight stress field increases (Figure 8c). The maximum horizontal principal stress generally shows an increasing trend with the increase in borehole depth. It is worth noting that, at the depth of −1050 m, the maximum horizontal principal stress shows a sudden increase, reaching 41.83 MPa. Under this high stress level, the core discing phenomenon occurs in the borehole, as shown in Figure 9. This finding indicates that the maximum horizontal principal stress undergoes unstable changes in this area and may have geological structural reasons underpinning this.

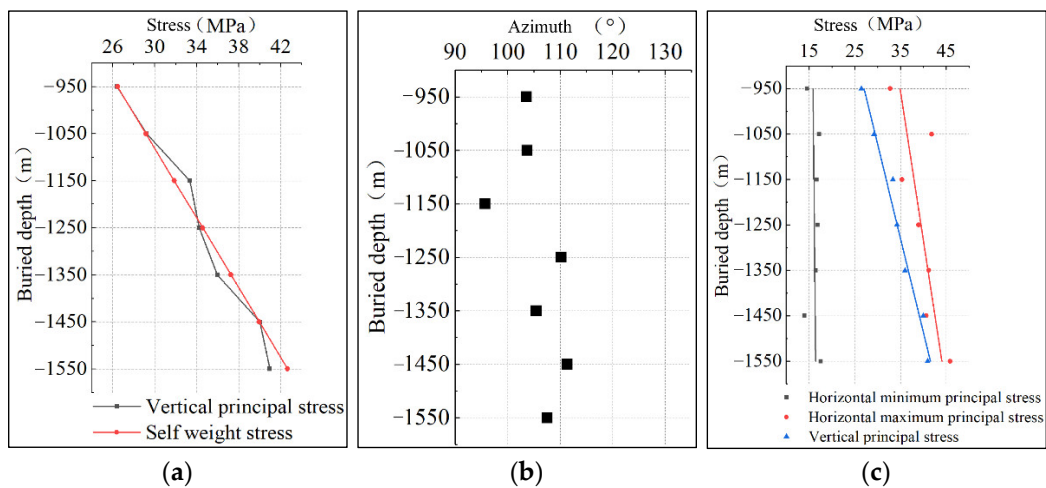


**Figure 8.** Distribution of in situ stress: (a) vertical principal stress; (b) azimuth; (c) horizontal principal stress.



**Figure 9.** Core discing phenomenon.

## 5. Comparison and Verification

To verify the accuracy of the in situ stress measurement by the core reorientation technology and the AE method, six measuring points were selected from a burial depth of  $-860$  m to  $-1060$  m in Xincheng Gold Mine, and the Swedish LUT in situ stress testing system was used for in situ stress measurement by the stress relief method, as shown in Figure 10. The results of in situ stress measurement are summarized in Figure 11.

The maximum horizontal principal stress, minimum horizontal principal stress, and vertical principal stress at each measuring point were calculated using the linear function fitting obtained from the AE method. The two sets of data were compared and analyzed, as shown in Table 3.

Figure 11 indicates that the inclination angle of the maximum principal stress  $\sigma_1$  at a depth of  $-860$  m is  $4.56^\circ$ , which is a horizontal stress. As the depth increases to  $-1060$  m, its inclination angle reaches  $13.75^\circ$ ; it remains a quasi-horizontal stress, but its vertical stress component increases significantly. It can be seen from the changing trend in  $\sigma_1$  that, as the depth increases, the effect of the stress in the vertical direction gradually increases. This is consistent with the data measured by the AE method. The azimuth angle of the maximum principal stress  $\sigma_1$  at each depth is between  $260.34^\circ$  and  $284.58^\circ$ , and the azimuth angle of the maximum horizontal principal stress measured by the AE method is between  $275.72^\circ$  and  $291.33^\circ$ . The azimuth angles of the maximum principal (or horizontal principal) stress measured by the two methods are similar.



**Figure 10.** Stress relief process: (a) drilling and cleaning; (b) installing strain gauge probe; (c) stress relief and data acquisition; (d) obtaining core tube; (e) confining pressure calibration; (f) in situ stress calculation.

**Table 3.** Data comparison between the two methods.

Depth (m)	Maximum Horizontal Principal Stress $\sigma_H$ (MPa)			Minimum Horizontal Principal Stress $\sigma_h$ (MPa)			Vertical Principal Stress $\sigma_v$ (MPa)		
	AE	Stress Relief	Deviation (%)	AE	Stress Relief	Deviation (%)	AE	Stress Relief	Deviation (%)
−860	27.815	33.110	−16.0	11.606	14.468	−19.8	23.713	21.345	+11.1
−860	27.815	32.374	−14.1	11.606	14.528	−20.1	23.713	21.688	+9.3
−925	29.687	35.292	−15.9	12.314	19.944	−38.3	25.479	25.079	+1.6
−970	30.983	36.788	−15.8	12.805	22.349	−42.7	26.690	26.919	−0.9
−1060	31.125	42.112	−26.1	13.786	16.856	−18.2	29.111	28.234	+3.1
−1060	31.125	41.803	−25.5	13.786	24.311	−43.3	29.111	29.128	−0.1

The three principal stresses measured by the stress relief method are listed in Table 3. After comparison with the results measured by the AE method, the principal stresses measured by the two methods are shown to be consistent, and the trends therein are in good agreement. The vertical principal stress error is the smallest, and the error is almost negligible. The average deviation of the maximum horizontal principal stress is −18.9%. The minimum horizontal principal stress error is relatively large, and the average deviation is −30.4%, which may be due to errors in the measurement process, complex geological conditions, and that the AE method does not consider shear stress. Although there are certain errors, the results measured using the two methods are acceptable.

In summary, the measured in situ stresses found using the combination of core orientation and the AE method are in good agreement with those measured by the stress relief method. In particular, the magnitude of the vertical principal stress, the azimuth angle of the maximum principal stress, and the trends in the three principal stresses are in good agreement.

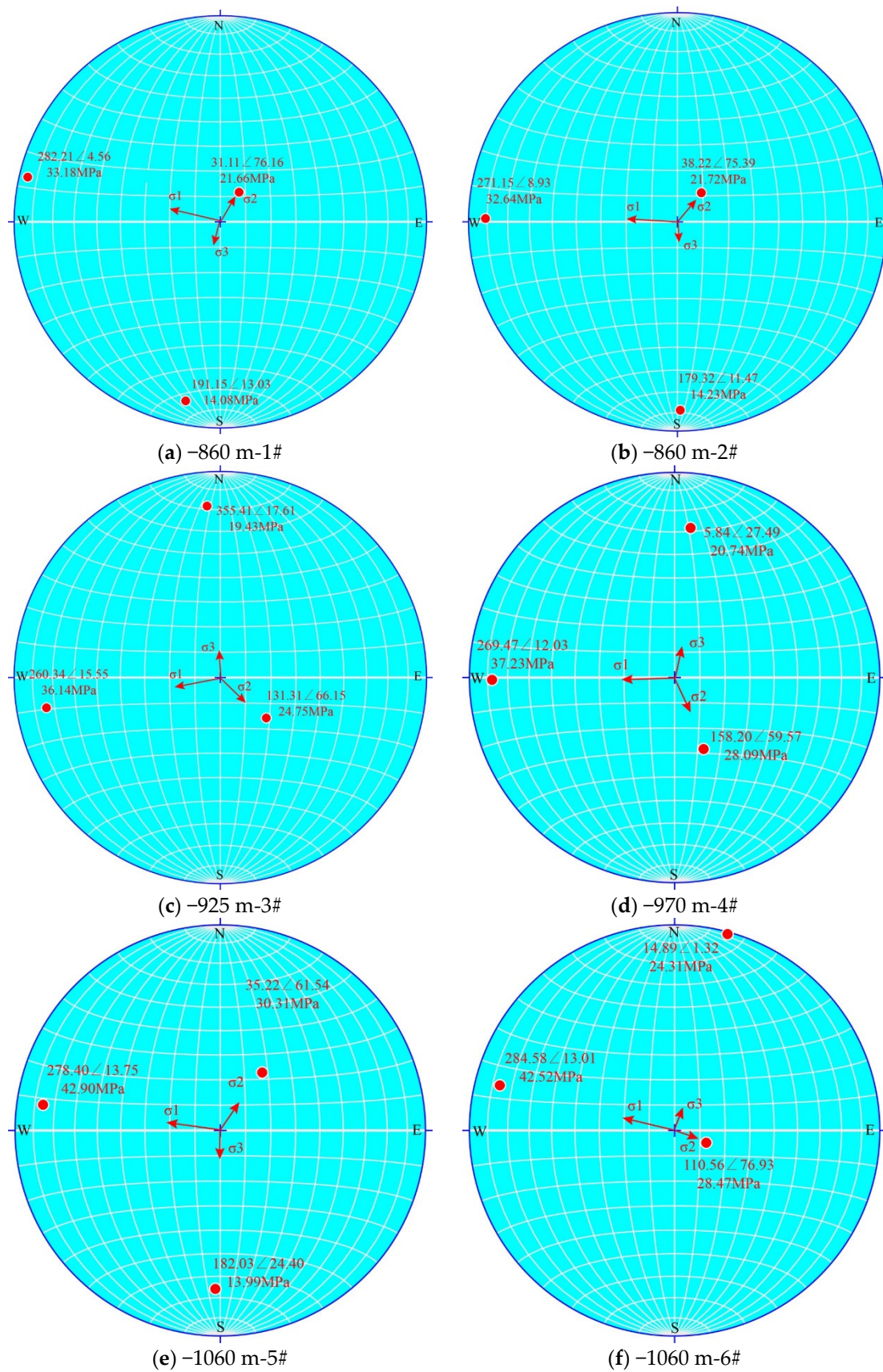


**Figure 11.** Stress relief method results: (a) 1# at depth of  $-860$  m; (b) 2# at depth of  $-860$  m; (c) 3# at depth of  $-925$  m; (d) 4# at depth of  $-970$  m; (e) 5# at depth of  $-1060$  m; (f) 6# at depth of  $-1060$  m.

## 6. Conclusions

A nonoriented geological core reorientation technique based on the drilling trajectory projection principle was proposed, and a core orientation system was established based on this technique. The system was used to reorient cores taken from ultradeep geological boreholes, and then the AE method was adopted to measure the in situ stress on these cores. The in situ stress measurement by the stress relief method was also conducted in a mining area where the ultradeep borehole was located, which could verify the reliability of the new technique. The following conclusions can be drawn:

- (1) The core in an ultradeep geological borehole was reoriented using the developed nonoriented geological core reorientation technology and test system. This technical method only requires the geological core as the test sample without redundant operation in the process of drilling. The utility model has the advantages of low cost, simple operation, and strong applicability.
- (2) To obtain the in situ stress distribution of the deepest shaft of Xincheng Gold Mine, the cores collected from a  $-1550$  m ultradeep geological borehole in the mining area were reoriented, and then the in situ AE stress measurement method was conducted. The measured results show that, as the depth increases, the in situ stress field gradually changes from one dominated by horizontal stress to one dominated by vertical stress; the vertical principal stress and the maximum horizontal principal stress increase with the increase in the burial depth. At a depth of  $-1550$  m, all of them exceed 40 MPa, reaching a high level of in situ stress; the azimuth angles of the maximum principal stress are all around  $283^\circ$ .
- (3) To verify the accuracy of the in situ stress results measured by the combination of the core orientation technology and the AE method, six measuring points were selected for in situ stress measurement by the stress relief method in Xincheng Gold Mine. The results imply that the three-dimensional in situ stress results measured by the two methods are in good agreement. This proves that the core orientation technology combined with the AE method is reliable in measuring the in situ stress in the area of interest.

**Author Contributions:** C.M. obtained funding support, conducted the field investigation, and wrote the article; G.T. conducted the experimental tests and processed the results of the experiment; X.L. obtained funding support and discussed the results; J.X. conducted the fieldwork and collected the core specimens; J.C. analyzed the principle of orientation, conducted the core orientation, and wrote the article. All authors have read and agreed to the published version of the manuscript.

**Funding:** This research was funded by the National Natural Science Foundation of China, Grant Numbers 52074352 and 51927808.

**Data Availability Statement:** Not applicable.

**Acknowledgments:** We highly appreciate the contribution of fieldwork from Xincheng Gold Mine and Deep Shaft Laboratory of Shandong Gold Group.

**Conflicts of Interest:** The authors declare no conflict of interest.

## References

1. Li, X.B.; Jian, Z.; Wang, S.F.; Bing, L. Review and practice of deep mining for solid mineral resources. *Chin. J. Nonferr. Metal.* **2017**, *27*, 1236–1262.
2. Cai, M.F.; Xue, D.L.; Ren, F.H. Current status and development strategy of metal mines. *Chin. J. Eng.* **2019**, *41*, 417–426.
3. Yan, Z.W.; Liu, D.G.; Wang, Z.L.; Zhao, D.M.; Tian, H.T. Research on the Method and Model for Calculating Impact Load in the Rockburst Tunnel. *Minerals* **2022**, *12*, 13. [[CrossRef](#)]
4. Gong, F.Q.; Luo, Y.; Li, X.B.; Si, X.F.; Tao, M. Experimental simulation investigation on rockburst induced by spalling failure in deep circular tunnels. *Tunn. Undergr. Space Technol.* **2018**, *81*, 413–427. [[CrossRef](#)]
5. Gong, F.Q.; Si, X.F.; Li, X.B.; Wang, S.Y. Experimental investigation of strain rockburst in circular caverns under deep three-dimensional high-stress conditions. *Rock Mech. Rock Eng.* **2019**, *52*, 1459–1474. [[CrossRef](#)]

6. Kaiser, P.K.; Cai, M. Design of rock support system under rockburst condition. *J. Rock Mech. Geotech. Eng.* **2012**, *4*, 215–227. [[CrossRef](#)]
7. Sousa, L.R.E.; Miranda, T.; Sousa, R.L.E.; Tinoco, J. The use of data mining techniques in rockburst risk assessment. *Engineering* **2017**, *3*, 552–558. [[CrossRef](#)]
8. Liu, B.; Zhu, Y.G.; Liu, Q.S.; Liu, X.W. A Novel in Situ Stress Monitoring Technique for Fracture Rock Mass and Its Application in Deep Coal Mines. *Appl. Sci.* **2019**, *9*, 3742. [[CrossRef](#)]
9. Wang, X.G.; Wang, J.D.; Hou, T.S. Geostress tests and analysis of the Tibet Bangpu mining area. *Int. J. Geotech. Eng.* **2017**, *11*, 156–161.
10. Goswami, D.; Hazarika, P.; Roy, S. In situ stress orientation from 3 km borehole image logs in the Koyna Seismogenic zone, Western India: Implications for transitional faulting environment. *Tectonics* **2020**, *39*, 17. [[CrossRef](#)]
11. Guo, H.J.; Ming, J.; Zhao, W.S. Analysis of the distribution characteristics and laws of in situ stress in China's coal mines. *Arab. J. Geosci.* **2020**, *13*, 14. [[CrossRef](#)]
12. Li, Y.; Fu, S.; Qiao, L.; Liu, Z.; Zhang, Y. Development of twin temperature compensation and high-level biaxial pressurization calibration techniques for CSIRO in-situ stress measurement in depth. *Rock Mech. Rock Eng.* **2019**, *52*, 1115–1131. [[CrossRef](#)]
13. Yang, W.; Lin, B.; Zhai, C.; Li, X.; Sun, X.; Zhang, C. A new technology for coal and gas control based on the in situ stress distribution and the roadway layout. *Int. J. Min. Sci. Technol.* **2012**, *22*, 145–149. [[CrossRef](#)]
14. Cao, A.; Jing, G.; Dou, L.; Wu, Y.; Zhang, C. Statistical analysis of distribution patterns of coal seams in fold zones in Northwest China. *Int. J. Min. Sci. Technol.* **2018**, *28*, 819–828. [[CrossRef](#)]
15. Zhou, Y.; Chen, X.; Fukushima, E.F.; Wu, M.; Cao, W.; Terano, T. An online hybrid prediction model for mud pit volume in the complex geological drilling process. *Control Eng. Pract.* **2021**, *111*, 104793. [[CrossRef](#)]
16. Li, Y.; Cao, W.; Hu, W.; Wu, M. Identification of downhole conditions in geological drilling processes based on quantitative trends and expert rules. *Neural Comput. Appl.* **2021**, 1–10. [[CrossRef](#)]
17. Deng, C.; He, H.; Pan, Y.; Zhu, R. Chronology of the terrestrial Upper Cretaceous in the Songliao Basin, northeast Asia. *Palaeogeogr. Palaeoclimatol. Palaeoecol.* **2013**, *385*, 44–54. [[CrossRef](#)]
18. Ge, K.; Liu, Q.; Deng, J.; Nobes, D.; Wang, Y.; Wang, Y.; Chen, X. Rock magnetic investigation and its geological significance for vein-type uranium deposits in southern China. *Geochem. Geophys. Geosynthesis* **2017**, *18*, 1333–1349. [[CrossRef](#)]
19. Li, Y.; Qiao, L.; Sui, Z. In-situ stress measurement based on acoustic emission in combination with core orientation techniques. In Proceedings of the ISRM International Symposium on In-Situ Rock Stress, Beijing, China, 25 August 2010; OnePetro: Richardson, TX, USA, 2010.
20. Bleakly, D.C.; Alstine, D.; Packer, D.R. Core orientation—1: Controlling errors minimizes risk and cost in core orientation. *Oil Gas J.* **1985**, *83*, 103–109.
21. Morris, A.; Gee, J.; Pressling, N.; John, B.; MacLeod, C.J.; Grimes, C.; Searle, R. Footwall rotation in an oceanic core complex quantified using reoriented Integrated Ocean Drilling Program core samples. *Earth Planet. Sci. Lett.* **2009**, *287*, 217–228. [[CrossRef](#)]
22. Davison, I.; Haszeldine, R. Orienting conventional cores for geological purposes: A review of methods. *J. Petrol. Geol.* **1984**, *7*, 461–466. [[CrossRef](#)]
23. Nelson, R.; Lenox, L.; Ward, B., Jr. Oriented core: Its use, error, and uncertainty. *AAPG Bull.* **1987**, *71*, 357–367.
24. Kessels, W.; Kück, J. Computer-aided matching of plane core structures with borehole measurements for core orientation. *Sci. Drill.* **1992**, *3*, 225–238.
25. MacLeod, C.; Parson, L.; Sager, W. Identification of tectonic rotations in boreholes by the integration of core information with Formation MicroScanner and Borehole Televiewer images. *Geol. Soc.* **1992**, *65*, 235–246. [[CrossRef](#)]
26. Paulsen, T.S.; Jarrard, R.D.; Wilson, T.J. A simple method for orienting drill core by correlating features in whole-core scans and oriented borehole-wall imagery. *J. Struct. Geol.* **2002**, *24*, 1233–1238. [[CrossRef](#)]
27. Jin-Chao, W.; Chuan-Ying, W.; Sheng, H.; Zeng-Qiang, H.; Yi-Teng, W. A new method for extraction of parameters of structural surface in borehole images. *Rock Soil Mech.* **2017**, *38*, 3074–3080.
28. Jin-Chao, W.; Chuan-Ying, W.; Xin-Jian, T.; Sheng, H.; Zeng-Qiang, H.; Yi-Teng, W. A method for estimating rock mass joint size using borehole camera technique. *Rock Soil Mech.* **2017**, *38*, 2701–2707.
29. Wang, J.; Tao, D.; Huang, Y.; Wang, C.; Han, Z.; Hu, S. Borehole imaging method based on ultrasonic synthetic aperture technology. *Rock Soil Mech.* **2019**, *40* (Suppl. 1), 557–564.
30. Haggas, S.; Brewer, T.; Harvey, P.; Iturrino, G. Relocating and orientating cores by the integration of electrical and optical images: A case study from Ocean Drilling Program Hole 735B. *J. Geol. Soc. Lond.* **2001**, *158*, 615–623. [[CrossRef](#)]
31. Shigematsu, N.; Otsubo, M.; Fujimoto, K.; Tanaka, N. Orienting drill core using borehole-wall image correlation analysis. *J. Struct. Geol.* **2014**, *67*, 293–299. [[CrossRef](#)]
32. Sugimoto, T.; Yamamoto, Y.; Yamamoto, Y.; Lin, W. A Method for Core Reorientation Based on Rock Remanent Magnetization: Application to Hemipelagic Sedimentary Soft Rock. *Mater. Trans.* **2020**, *61*, 1638–1644. [[CrossRef](#)]
33. Lackie, M.; Schmidt, P. Drill core orientation using palaeomagnetism. *Explor. Geophys.* **1993**, *24*, 609–613. [[CrossRef](#)]
34. Butler, R.F.; Butler, R.F. *Paleomagnetism: Magnetic Domains to Geologic Terranes*; Blackwell Scientific Publications: Boston, MA, USA, 1992; Volume 319.
35. Tauxe, L. *Essentials of Paleomagnetism*; University of California Press: Los Angeles, CA, USA, 2010.

36. Dong, P. Orientation determination of maximum horizontal stress in reservoir formation by paleomagnetic orientation of cores. *Chin. J. Rock Mech. Eng.* **2004**, *23*, 2480–2483.
37. Villaescusa, E.; Seto, M.; Baird, G. Stress measurements from oriented core. *Int. J. Rock Mech. Min. Sci.* **2002**, *39*, 603–615. [[CrossRef](#)]
38. Zhao, X. Application of the Kaiser effect of acoustic emission to measure vertical stress in an underground mine. *Insight* **2012**, *54*, 662–666. [[CrossRef](#)]
39. Lavrov, A. The Kaiser effect in rocks: Principles and stress estimation techniques. *Int. J. Rock Mech. Min. Sci.* **2003**, *40*, 151–171. [[CrossRef](#)]
40. Tuncay, E.; Obara, Y. Comparison of stresses obtained from acoustic emission and compact conical-ended borehole overcoring techniques and an evaluation of the Kaiser Effect level. *Br. Eng. Geol. Environ.* **2011**, *71*, 367–377. [[CrossRef](#)]
41. Lehtonen, A.; Cosgrove, J.W.; Hudson, J.A.; Johansson, E. An examination of in situ rock stress estimation using the Kaiser effect. *Eng. Geol.* **2012**, *124*, 24–37. [[CrossRef](#)]
42. Chen, Y.; Irfan, M.; Song, C. Verification of the Kaiser Effect in rocks under tensile stress: Experiment using the brazilian test. *Intl. J. Geomech.* **2018**, *18*, 04018059. [[CrossRef](#)]
43. Chen, Y.; Meng, Q.; Li, Y.; Pu, H.; Zhang, K. Assessment of appropriate experimental parameters for studying the Kaiser effect of rock. *Appl. Sci.* **2020**, *10*, 7324. [[CrossRef](#)]
44. Kharghani, M.; Goshtasbi, K.; Nikkah, M.; Ahangari, K. Investigation of the Kaiser effect in anisotropic rocks with different angles by acoustic emission method. *Appl. Acoust.* **2021**, *175*, 107831. [[CrossRef](#)]
45. Fu, X.; Ban, Y.X.; Xie, Q.; Abdullah, R.A.; Jun, D. Time delay mechanism of the Kaiser effect in sandstone under uniaxial compressive stress conditions. *Rock Mech. Rock Eng.* **2021**, *54*, 1091–1108. [[CrossRef](#)]
46. Li, C.; Nordlund, E. Experimental verification of the Kaiser effect in rocks. *Rock Mech. Rock Eng.* **1993**, *26*, 333–351. [[CrossRef](#)]
47. Lubinski, A. A study of the buckling of rotary drilling strings. *Drill. Prod. Pract.* **1950**, 178–214.
48. Lavrov, A.; Vervoort, A.; Wevers, M.; Napier, J.A.L. Experimental and numerical study of the Kaiser effect in cyclic Brazilian tests with disk rotation. *Int. J. Rock Mech. Min. Sci.* **2002**, *39*, 287–302. [[CrossRef](#)]
49. Ding, Y.; Zhang, D. Application of the incomplete erosion phenomenon in acoustic emission activities to the measurement of geostress. *Chin. J. Rock Mech. Eng.* **1991**, *10*, 313–326.
50. Boyce, G.M.; McCabe, W.M.; Koerner, R.M. Acoustic emission signatures of various rock types in unconfined compression. *Astm Spec. Tech. Publ.* **1981**, *750*, 13.
51. Bai, X.; Zhang, D.; Wang, H.; Li, S.; Rao, Z. A novel in situ stress measurement method based on acoustic emission Kaiser effect: A theoretical and experimental study. *R. Soc. Open Sci.* **2018**, *5*, 181263. [[CrossRef](#)] [[PubMed](#)]
52. Goodno, B.J.; Gere, J.M. *Mechanics of Materials*; Cengage Learning: Boston, MA, USA, 2020.